HHS Public Access

Author manuscript

J Orthop Res. Author manuscript; available in PMC 2024 December 01.

Published in final edited form as:

J Orthop Res. 2023 December ; 41(12): 2599–2609. doi:10.1002/jor.25627.

Development and Expansion of Intramuscular Adipose Tissue is Not Dependent on UCP-1-Lineage Cells in Mice

Jacob C. Parson[1], **Xiao Zhang**[2,4], **Clarissa S. Craft**[2,6], **Kristann L. Magee**[2], **Erica L. Scheller**[2,4,6], **Gretchen A. Meyer**[1,3,4,5]

[1]Program in Physical Therapy, Washington University, St. Louis, MO

[2]Division of Bone and Mineral Diseases, Department of Medicine, Washington University, St. Louis, MO

[3]Department of Orthopedic Research, Washington University, St. Louis, MO

[4]Department of Biomedical Engineering, Washington University, St. Louis, MO University, St. Louis, MO

[5]Department of Neurology, Washington University, St. Louis, MO

[6]Department of Cellular Biology and Physiology, Washington University, St. Louis, MO

Abstract

Accumulation of adipose tissue within and outside of skeletal muscle is associated with orthopaedic injury and metabolic disease, where it is thought to impede muscle function. The close juxtaposition between this adipose and myofibers has led to hypotheses that paracrine interactions between the two regulate local physiology. Recent work suggests that intramuscular adipose tissue (IMAT) may have features of beige or brown fat, indicated by expression of uncoupling protein-1 (UCP-1). However, this is contested by other studies. Clarification of this point is needed to inform our understanding of the relationship between IMAT and muscle health. To achieve this, we examined the effects of constitutive UCP-1+ cell ablation (UCP1-DTA) on IMAT development and homeostasis. IMAT developed normally in UCP1-DTA mice, with no significant differences in quantity compared with wildtype littermates. Likewise, IMAT accumulation in response to glycerol induced injury was similar between genotypes, with no significant differences in adipocyte size, quantity or dispersion. This suggests that neither physiological nor pathological IMAT express UCP-1 and that the development of IMAT does not depend on UCP-1 lineage cells. In response to β3-adrenergic stimulation, we find minor, localized UCP-1 positivity in wildtype IMAT, but the bulk of the adipocytes are unresponsive. In contrast, two depots of muscle-adjacent (epi-muscular) adipose tissue have reduced mass in UCP1-DTA mice and UCP-1 positivity in wildtype littermates, comparable to traditional beige and

4444 Forest Park Blvd., St. Louis MO, 63108, Phone: 314-286-1425, Fax: 314-767-0674, meyerg@wustl.edu.

Authors Contributions Statement:

J.C.P., X.Z., E.L.S., and G.A.M. were responsible for the conception and design of the study. J.C.P., X.Z., C.S.C., K.L.M., E.L.S., and G.A.M. contributed to the acquisition, analysis, and interpretation of the data. J.C.P. and G.A.M. were responsible for the drafting of the manuscript and X.Z. and E.L.S. contributed to critical revision of the manuscript. All authors have read and approved the final version of the manuscript and agree to be accountable for all aspects of the work in ensuring that questions related to the accuracy or integrity of any part of the work are appropriately investigated and resolved. All persons designated as authors qualify for authorship, and all those who qualify for authorship are listed.

brown adipose depots. Taken together this evidence strongly supports a white adipose phenotype for mouse IMAT and a brown/beige phenotype for some adipose outside the muscle boundary.

Introduction

Traditionally, adipose is identified in two subtypes: white (WAT) and brown adipose tissue (BAT). These subtypes differ distinctly by appearance, morphology, gene expression, and metabolism[1]. Whereas WAT stores energy in the form of lipids, BAT dissipates energy through a specialized mitochondrial protein known as uncoupling protein-1 (UCP-1), that has become the quintessential marker of BAT[2]. The unique attributes of BAT also extend beyond thermogenesis to include paracrine/endocrine signaling which is thought to be beneficial in many aspects of health[3]. In the last decade, the field has come to appreciate the role of adipose signaling in whole-body physiology. However, more recent work has further revealed diverse roles of unique fat depots located throughout the body and identified a thermogenic spectrum between BAT and WAT, frequently referred to as beige fat.

Skeletal muscle has two general locations of adjacent adipose: one outside of the muscle fascial boundary called inter-muscular or epi-muscular adipose tissue (EMAT) and the other within the fascial boundary between myofibers called intra-muscular adipose (IMAT). These depots have been the subject of extensive research in humans as their expansion is associated with muscle dysfunction and poor physical performance across a host of disorders[4]. However, the exact definition of IMAT is not consistent throughout the literature and many studies combine EMAT and IMAT into a single depot despite their anatomical separation[4]. Findings differ on the phenotype of EMAT and IMAT as some claim that muscle-associated fat is brown or beige, while others do not. Specifically, at least two EMAT depots have been suggested to be UCP-1 positive and thermogenic: EMAT adjacent to femoral muscle (also referred to as femoral BAT)[5] and EMAT adjacent to the rotator cuff (also referred to as axillary BAT)[6; 7]. However, findings as to the phenotype of IMAT are more controversial. Injury-induced models of IMAT including glycerol[8] and cardiotoxin[9] in mouse tibialis anterior muscle shows increased UCP-1 expression in conjunction with IMAT accumulation. Stimulation of cultured IMAT precursor cells, fibro/adipogenic progenitors (FAPs) with β3-adrenergic agonist also increased UCP-1 expression, suggesting that these cells were the source of the in-vivo results[8]. However, some other studies suggest that IMAT and FAP expression of UCP-1 may be dependent on mouse strain as UCP-1 expression is found in IMAT of Sv/129 strain, yet absent in C57Bl/6 mice[8; 10]. Similarly, Pisani et al. characterized IMAT as white in B6D2 mice and Liu et al., using a mixed Sv/129 and C57Bl/6 background, found that IMAT was derived from a different developmental lineage than BAT[11]. In humans, FAPs derived from fetal muscle are capable of brown adipogenic differentiation and UCP-1 expression[12], but those from obese adults display the phenotype and metabolic properties of white adipose tissue[12; 13]. This conflicting evidence suggests that UCP-1 expression in IMAT may depend on age, genetic, or metabolic factors.

Due to the association of IMAT with poor skeletal muscle function in a vast array of diseases and injuries, it is a tantalizing therapeutic target. Therefore, defining the phenotype of IMAT will be valuable in developing IMAT-targeted therapeutics. Some evidence suggests that

UCP-1 expression in IMAT is beneficial to local muscle. Mice with increased muscular UCP-1 expression are protected from obesity with improvements in glucose disposal and increased energy expenditure[10]. As well, exogenous transplant of UCP-1 positive adipocytes or progenitors may aid in muscle healing and regeneration[14; 15]. Conversely, the loss of UCP-1 expression in IMAT precursor cells may parallel comorbidities, such as obesity and diabetes[12; 13]. However, as IMAT is difficult to isolate and study, most evidence for UCP-1 positivity comes from the study of progenitor cells *in vitro* or immunostaining of histological sections. This is a substantial limitation, as initial evidence of UCP-1 expression in other fat depots such as bone marrow adipose tissue (BMAT) by these methods has been refuted by more sophisticated methods[16].

To address the conflicting evidence regarding the phenotype of IMAT, we generated and characterized a unique transgenic mouse model in which UCP-1-expressing cells are constitutively ablated. Using this model, we then evaluated whether naturally occurring or injury-induced IMAT expresses UCP-1 or derives from UCP-1-lineage cells by examining whether it succumbed to ablation. We additionally explored whether IMAT responds to β3 adrenergic "browning" stimulation by upregulation of UCP-1 followed by cell death. We show that development of IMAT both naturally and in response to injury does not require UCP-1-lineage cells. However, we find that wild type IMAT is responsive to β3 adrenergic stimulation and a small subset of intramuscular adipocytes inducibly express UCP-1. Together, this suggests a predominantly white phenotype for IMAT in mice at baseline with a minimal capacity for "browning" in select contexts.

Methods

Ethical approval

All procedures were performed in accordance with the National Institutes of Health's Guide for the Use and Care of Laboratory Animals and were approved by the Animal Studies Committee of the Washington University School of Medicine.

Experimental Design

Experiments were performed on 3–6 month-old male and female UCP1-DTA mice (generated as previously described[17]) and littermate controls. Briefly, UCP1-DTA mice were created by crossing transgenic mice with homozygous lox-stop-lox-ROSA-diphtheria toxin fragment A (DTA) gene (The Jackson Laboratory: 010527 or 009669) with mice expressing Cre recombinase under control of the UCP-1 promoter (The Jackson Laboratory: 024670), causing cells with sufficient UCP-1 expression to co-express DTA and die. Data from the UCP1-DTA strains were combined for this collaboration. Body, liver and adipose masses were not different between strains (Supplemental Figure 1), and both strains exhibited similar phenotypic appearance and behavior. All experiments were performed during the light (inactive phase). All mice were housed at thermoneutrality (30°C) with free cage activity and *ad libitum* access to food and water.

Intramuscular Injection

Glycerol injections were delivered to either the mid-belly of the extensor digitorum longus (EDL) muscle or tibialis anterior (TA) muscle to induce regeneration with infiltration of IMAT, as previously described[18]. The contralateral EDL was injected with saline. Briefly, mice were anesthetized with 2% inhaled isoflurane at 2 L min^{-1} and the EDL was exposed through a 2mm skin incision. 10 μL of either glycerol (50% v/v; Sigma Aldrich, St. Louis, MO), or sterile saline (10 μL) was then injected into the mid-belly of the EDL. For TA injections, 50 μL of glycerol or saline was injected into the mid-belly of the TA. Skin incisions were closed with suture glue and mice were given analgesia and allowed free cage activity until the experimental end-point.

CL316,243 treatment

A subset of mice with intramuscular glycerol injection in the TA was randomized to saline or CL316,243 treatment 4 weeks post-injection as previously described [16]. Briefly, mice were subjected to eight days of consecutive subcutaneous injections of 100 μL of either CL316,243 (0.03 mg/kg body mass) or saline followed by sacrifice and tissue harvest. Tissues collected for “beiging” analysis include epididymal white adipose (Epi.), inguinal subcutaneous white adipose (Ing.), classical interscapular brown fat (BAT), Axillary epi-muscular fat (EMAT) located near the rotator cuff, femoral (Fem.) EMAT located near the gluteal region, and induced IMAT within TA muscles.

IMAT Quantification

Identification and quantification of fatty infiltration was assessed as previously described[19]. Briefly, tissues were decellularized in a 1% solution of sodium dodecyl sulfate (SDS; Sigma Aldrich, St. Louis, Mo), fixed in 3.7% formaldehyde for 48 h and then incubated with the lipid soluble dye BODIPY (0.05 mg ml^{-1} 493/503; Life Technologies, Carlsbad, CA) or Oil Red O (ORO, Sigma Aldrich, St. Louis, MO). An Olympus FV1200 scanning confocal microscope was used to image BODIPY through the muscle volume. ImageJ software (NIH, Bethesda, MD) was used to quantify individual adipocyte regions of interest (ROI) and these were analyzed in a semi-automated segmentation process to quantify the total number of adipocytes, average adipocyte volume, total lipid volume and nearest neighbor index. ORO-stained muscles were imaged for qualitative assessment using a dissecting microscope (Zeiss, Oberkoshen, Germany) and ORO was quantified by the optical density of isopropanol extracted lipid (Synergy II, Bio-Tek, Winooski, VT).

Histological Processing

TA muscle specimens were flash frozen in isopentane cooled with liquid nitrogen and sectioned axially at 10μm with a cryostat (Leica Biosystems, Wetzlar, Germany). Sections were stained with hematoxylin and eosin (H&E) to visualize tissue morphology and ORO to visualize lipid accumulation (Biltz & Meyer, 2017). Sections were also immunostained against myosin heavy chain isoforms (MHC) isoforms type I, type IIa and type IIb (1:30; BA-F8, SC-71, BF-F3; Developmental Studies Hybridoma Bank, Iowa City, IA), and counterstained against laminin (1:400; ab11575; Abcam, Cambridge, UK) to quantify fiber types and areas. Fiber areas were typed and quantified using a custom

thresholding-based macro in Image J (NIH, Bethesda, MD). UCP-1 immunostaining was performed as previously described on fixed and paraffin embedded tissues[16]. Briefly, de-paraffinized sections were permeabilized and blocked with Vectastain Elite ABC kit (Vector Laboratories) followed by overnight incubation with anti-UCP-1 (1:2,000; ab10983; Abcam, Cambridge, UK) at 4°C. The next day, samples were washed, quenched of endogenous peroxidases, and stained with secondary antibody (ImPRESS) according to manufacturer's instructions. Finally, sections were incubated with DAB substrate for staining development and counterstained with hematoxylin.

Micro-Computed tomography

Tibia lengths were measured with digital calipers. After post-fixation in 10% neutral buffered formalin (NBF; Fisher Scientific 23–245684) for 24-hours, tibiae were washed with PBS and embedded in 2% agarose prior to scanning at 20μm voxel resolution with a Scanco μCT 40 (Scanco Medical AG). Analysis was performed using the micro-CT evaluation system according to reported guidelines[20]. For cortical bone, a region of 20 slices (400μm) positioned 2mm proximal to the tibia–fibula junction was analyzed at a threshold of 260 (on a 0–1000 scale relative to a pre-calibrated hydroxyapatite phantom). For trabecular bone, 100 slices (2mm) distal to the growth plate were contoured and analyzed at a threshold of 175.

PhenoMaster

To compare activity of the mice between genotypes, a PhenoMaster (TSE Systems) Metabolic Cage System was used. Activity was measured in the light phase by infrared sensor in the x, y and z planes over 60 minutes following a 24-hour acclimatization period.

Statistical Analysis

Grouped data were analyzed by independent t-test or two-way analysis of variance (ANOVA) with Tukey's post hoc comparisons test to determine statistical differences. Data were tested for normality using D'Agostino-Pearson and Shapiro-Wilk testing. All statistical analyses were run with GraphPad Prism (San Diego, CA). Statistical significance set at $p<0.05$.

Results

UCP1-DTA Mice Have Reduced Body and Adipose Masses Compared to WT Mice

We first sought to characterize the baseline phenotype of the UCP1-DTA mouse. From weaning, UCP1-DTA mice are visibly smaller than WT mice (Fig. 1A). Quantification of body mass revealed a 20% reduction in female and 25% reduction in male UCP1-DTA mice compared with WT across the ages tested. Analysis by 2-way ANOVA found significant main effects for age and genotype (Fig. 1B). When normalized to body mass, there were few differences in organ masses between genotypes (Fig. 1C–F) – notably only a main effect for sex and genotype for normalized heart mass with UCP1-DTA mice having significantly larger hearts (Fig. 1C) and a main effect for sex and genotype and a significant sex-genotype interaction with female UCP1-DTA mice having significantly smaller spleens (Fig. 1F). As deletion of UCP-1- expressing cells is expected to impact adipose tissue,

we further analyzed the effect of genotype in five adipose depots (illustrated in Fig. 1G). Overall, both female (Fig. 1H) and male (Fig. 1I) UCP1-DTA mice had significantly smaller normalized adipose masses compared with WT with main effects for both adipose depot and genotype and a significant depot-genotype interaction. As expected, the degree of depot mass reduction was highest in the depots with the highest UCP-1 expression as measured by qPCR (Supplemental Figure 2). Notably, classical brown fat depots including interscapular BAT and epi-muscular axillary fat were effectively eliminated. By contrast, the mass of inducible-brown fat depots with intermediate UCP-1 expression such as inguinal WAT and femoral IMAT was reduced by approximately 39% and 53%, respectively.

In addition to this, we found that even epididymal fat with low or absent UCP-1 expression was decreased. This unexpected reduction could derive from a head tilt and circling phenotype whereby the UCP1-DTA mice were commonly found ambulating in rapid circles within their cage (Supplemental Video). To quantify these patterns, we performed activity assessments of WT and UCP1-DTA mice. We found that both male and female UCP1-DTA mice had significant increases in x-y plane movement with less rearing into the z-plane during the 60-minute assessment period (Figs. 1J–1M). This overall increase in movement may contribute to the partial decrease in size of the white and inducible-brown fat depots, in addition to any effects due to UCP1-DTA mediated cell death.

UCP1-DTA Mice Have Altered Skeletal Muscle and Bone Growth

To determine if ablation of UCP-1-expressing cells impacted musculoskeletal development, we performed morphometric analysis of skeletal muscle and bone. While slow-twitch (e.g. soleus) muscles were visually similar in size, fast-twitch (e.g. TA) muscles were grossly smaller in UCP1-DTA mice compared with WT (Fig. 2A). Consistent with this, raw muscle mass was significantly reduced in UCP1-DTA mice across muscles of the upper and lower limb and the diaphragm, except for the soleus (Fig. 2B). However, there was no deficit in relative muscle mass normalized to body mass, suggesting that muscle masses are reduced proportionally to body size. To assess changes at the cellular level, muscles were cryosectioned and immunostained for myosin heavy chain isoforms (Fig. 2C). No gross changes in morphology or structure were evident in any sections. Specific analysis of fiber cross-sectional area using 2-way ANOVA identified main effects of genotype in fast glycolytic Type IIb fibers only. Taken together, these data indicate that muscle mass is reduced proportionately to body mass, accomplished primarily through a reduction in type 2b fast fiber cross-sectional area, with preservation of structural morphology.

Consistent with the decrease in body size, UCP1-DTA mice had minor reductions in tibia length (Fig. 2E and F). In addition, UCP1-DTA mice had lower total cortical area, cortical thickness, and polar moment of inertia (pMOI) compared with WT. The decreases of cortical bone parameters were generally less prominent in female mice than in male mice, leading to a significant main effect of sex by 2-way ANOVA across parameters (Fig. 2G–2I). In contrast to cortical bone, trabecular bone volume fraction was slightly increased in both male and female UCP1-DTA mice (Fig. 2J). However, changes in trabecular bone number and thickness did not meet the threshold for significance (Fig. 2K–2L). Changes in bone of

the UCP1-DTA mice likely derive from the decreased body size and increased activity of the animals, respectively, in addition to any effects related to UCP1+ cell ablation.

Intramuscular adipose tissue (IMAT) develops without UCP-1-lineage cells

As UCP1-DTA effectively eliminated brown adipose and significantly reduced inducible-brown adipose mass, we next wanted to determine its effect on IMAT quantity. As IMAT cannot be reliably dissected and weighed, we utilized a decellularization protocol with ORO staining to approximate the volume of IMAT. Visual inspection revealed qualitatively similar amounts of IMAT between WT and UCP1-DTA genotypes across muscles (Fig. 3A). Similarly, quantification of ORO density in lipid extractions found no differences in lipid content between WT and UCP1-DTA genotypes across the four different muscles (Fig. 3B). This suggests that IMAT development in mice occurs via a mechanism that does not require UCP-1-lineage cells. Similarly, this suggests that upregulation of UCP-1 expression during adipocyte differentiation does not occur in IMAT in states of health.

UCP-1-lineage cells are not required for IMAT expansion after glycerol injury

IMAT deposition is frequently studied in a glycerol injection model [21]. Thus, we next wanted to examine whether glycerol injection would induce IMAT through the upregulation of UCP-1-expressing cells. Qualitatively, injection of glycerol into the TA induced comparable deposition of IMAT in both WT and UCP1-DTA mice (Fig. 4A–B). We next assessed whether the cellular morphometry of IMAT was affected by UCP-1 lineage cell ablation using fluorescent BODIPY staining and confocal microscopy on decellularized muscles. Decellularized muscles also illustrated robust accumulation of IMAT with glycerol treatment in both WT and UCP1-DTA strains at the macro (Fig. 4C) and micro (Fig. 4D) scale. There were no significant differences between WT and UCP1-DTA glycerol treated EDLs in total number of adipocytes (Fig. 4E), average volume of adipocytes (Fig. 4F), total lipid volume (Fig. 4G) or the distribution of intramuscular adipocytes as quantified using the nearest neighbor index (Fig. 4H). These results indicate in our mouse model that injury-induced fatty infiltration also does not depend on UCP-1-expressing cells.

Effects of CL316 Treatment on Adipose Depots

To further delineate the phenotype of IMAT, we injected the TA muscles of both hindlimbs of WT and UCP1-DTA mice with glycerol, waited 4 weeks for IMAT to develop and then treated mice with CL316,243 (CL316), a β3-adrenergic agonist that increases expression of UCP-1 in brown and inducible-brown adipose tissue depots[16]. As expected, CL316 treatment increased the multilocular morphology and UCP-1 immunostaining intensity in WT BAT and inguinal WAT (Fig. 5A; **rows 1–2**). As expected, this increased staining intensity was nearly absent in CL316 treated UCP1-DTA inguinal WAT. IMAT from saline treated mice was UCP-1-negative with unilocular morphology, but treatment with CL316 induced some localized UCP-1-positivity in WT mice (Fig. 5A; **row 3**), indicating that IMAT does have a limited capacity for stimulation-induced browning. UCP-1-positivity was largely absent in CL316 treated UCP1-DTA mice. By contrast, both WT femoral and axillary EMAT robustly responded to CL316 treatment with dramatically increased UCP-1-expression (Fig. 5A; **rows 4–5**). Similar to inguinal WAT, femoral EMAT from

UCP1-DTA had a dramatically blunted response. IMAT quantity in the diaphragm and TA, as measured by the optical density of extracted ORO staining in decellularized muscles, was not significantly affected by CL316 treatment (Fig. 5B).

Discussion

In this study, we demonstrate that UCP-1-lineage cells are not required for the development of IMAT or for its expansion in response to injury in mice. Additionally, we show that the maintenance of IMAT density and morphology does not depend on UCP-1 expression in mature adipocytes. This is based on a unique mouse model in which UCP-1+ cells are genetically ablated (UCP1-DTA), leading to loss of classical brown fat depots and reduced mass of beige WAT. In contrast, we find no effect of UCP1-DTA on IMAT, across multiple muscles of the upper and lower body, naturally occurring and injury-induced, both qualitatively and quantitatively at the level of the whole muscle and individual adipocyte. While histological analysis suggests that IMAT is capable of β3-adrenergic stimulation-induced browning, the response is muted compared with the traditional inguinal “beige” depot. Thus, this study indicates that IMAT has resident cells capable of UCP-1 expression but does not rely on them for development or expansion.

While the UCP1-DTA mouse model has been studied in the context of adipose signaling and metabolic derangement[22; 23], its musculoskeletal phenotype has not been extensively characterized. Our UCP1-DTA mice have complete elimination of the classical interscapular brown fat depot as well as a reduction in mass of other adipose depots which correlates with the degree of WT UCP-1 expression. Beyond this, we also noted interesting differences in activity between genotypes which could affect adipose mass. Specifically, UCP1-DTA mice are significantly more active than WT littermates due to a “circling” phenotype. We hypothesize that this behavior is due to deletion of UCP-1 expressing cells in the inner ear[24]. These observations differ from those previously reported in UCP1-DTA models, where only 60–70% BAT ablation was observed and mice become obese in adulthood.[22; 23] The reasons for these phenotypic discrepancies are unknown, but likely derive from a more robust deletion of UCP-1-expressing cells in our model. It is notable that previous studies used the FBV/N background, rather than C57Bl6 as used in this study, and genetic differences may underlie this difference in efficiency.

A strength of our study is the comprehensive assessment of IMAT. With this, we were unable to detect differences between UCP1-DTA and WT IMAT by gold-standard histological assessment, decellularization with ORO staining or individual adipocyte metrics assessed with confocal microscopy. These results indicate that UCP-1-expressing cells are not necessary for the development or pathological accumulation of IMAT in mouse muscle. In support of this, the majority of IMAT in both WT and UCP1-DTA mice was characterized by unilocular adipocytes negative for UCP-1. While WT glycerol-injected TA muscles challenged with CL316 show isolated pockets of multilocular, UCP-1+ adipocytes, these were rare in comparison to the increased UCP-1 expression in the classical mouse beige inguinal WAT. These findings align with those published by Gorski et al. who also found UCP-1 positivity in CL316 treated glycerol-injected TAs from the Sv/129 strain[15; 25], but

also suggests that this is a supraphysiological phenomenon and UCP-1 expression is not typical of IMAT at baseline or in response to injury.

There is more compelling evidence for UCP-1 expression in FAPs than in mature IMAT adipocytes where a subpopulation of UCP-1+ FAPs have been identified by genetic lineage tracing[26] in absence of exogenous stimulation. This is surprising because UCP-1 is typically considered a marker of mature brown/beige adipocytes that is largely absent in pre-adipocytes and because mature IMAT appears to express little to no UCP-1. It is possible that these UCP-1+ FAPs are involved in another aspect of muscle physiology[15] and are not the FAP subpopulation that differentiate into IMAT or that the level of UCP-1 expression is sufficiently low to evade DTA mediated cell death and be undetectable by traditional immunostaining. The latter is supported by single cell and single nuclei RNAseq which does not detect UCP-1 transcripts in FAPs either during development or following injury[27; 28]. Additionally, recent evidence suggests that migratory adipose stromal cells from beige subcutaneous fat are capable of engrafting in regenerating muscle, augmenting the FAP population[29]. Whether these cells retain the capacity to differentiate into a beige adipocyte in muscle remains to be tested.

While our data strongly support a non-beige phenotype for IMAT in mice, some limitations should be considered. First, the UCP1-DTA genetic model may spare some cells with very low or transient UCP-1 expression. These findings are similar to Craft, et al. using the same UCP1-DTA mouse model, which detected the limited presence of UCP-1+ cells in the Inguinal WAT of UCP1-DTA mice[16]. Second, we did not evaluate the dependence of IMAT on UCP-1-lineage cells across mouse strains. Other strains, Sv/129 in particular, may rely more heavily on the UCP-1 lineage in the generation of IMAT. The critical question, which we cannot answer here, is which strain is a better model of human IMAT. The data that we have so far suggest that adult human IMAT precursors express little UCP-1 at baseline and are relatively insensitive to β3-adrenergic stimulation[12; 13]. Finally, use of acute, injury-induced glycerol injection is not representative of models of chronic fatty infiltration such as that of Duchenne Muscular Dystrophy (DMD) or sarcopenia and the intersection of these models and UCP-1+ cell ablation will be an interesting avenue for future study.

In this study we also highlight that EMAT depots are anatomically and phenotypically distinct from IMAT, noted both by basal UCP-1 expression and response to CL316 treatment. These results align with those of Lehnig et al. and Meyer et al. who have found that in both rodents and humans, respectively, the axillary fat depot located near the rotator cuff has elevated UCP-1 expression[6; 7], and those of Wang et al. that show UCP-1 reporter activity in femoral EMAT [5]. The definition of EMAT is inconsistent at best and it is poorly characterized, but it has been noted throughout the human body, typically classified as *inter*-muscular adipose tissue. The fact that EMAT from two anatomically distinct regions in the C57Bl/6 expresses high levels of UCP-1 at baseline raises an interesting question as to its function. Fat transplant data from Bryniarski et al. suggest that brown fat outside the fascial boundary can impact muscle regeneration through paracrine signaling opening the intriguing possibility for EMAT-muscle crosstalk[14], a mechanism that has long been hypothesized for IMAT.

In summary, our results indicate that UCP-1-lineage cells are not required for the fatty infiltration of muscle, suggesting that the baseline phenotype of IMAT resembles WAT rather than beige or brown adipose tissue. However, we do find a few multilocular, UCP-1+ IMAT adipocytes in response to CL316 treatment indicating a limited capacity of IMAT to respond to “browning” stimuli. In contrast, we found that both at baseline and during external stimulation, EMAT depots located outside of the muscle border resemble a beige or BAT phenotype. A number of current therapeutic strategies are aimed at stimulating IMAT and precursor FAPs to upregulate UCP-1. Our findings in EMAT suggest this adipose as an additional, and potentially more responsive, target of these therapies.

Supplementary Material

Refer to Web version on PubMed Central for supplementary material.

Acknowledgments

This work was supported by R01AR075773 and R21AR071582 to GAM, R56AR081251 to ELS and NIH P30AR057235. The authors have no conflicts of interest to disclose.

References

1. Giralt M, Villarroya F. 2013. White, brown, beige/brite: different adipose cells for different functions? Endocrinology 154:2992–3000. [PubMed: 23782940]
2. Villarroya F, Cereijo R, Villarroya J, et al. 2017. Brown adipose tissue as a secretory organ. Nat Rev Endocrinol 13:26–35. [PubMed: 27616452]
3. Kajimura S, Spiegelman BM, Seale P. 2015. Brown and Beige Fat: Physiological Roles beyond Heat Generation. Cell Metab 22:546–559. [PubMed: 26445512]
4. Addison O, Marcus RL, Lastayo PC, et al. 2014. Intermuscular fat: a review of the consequences and causes. Int J Endocrinol 2014:309570. [PubMed: 24527032]
5. Wang H, Willershäuser M, Karlas A, et al. 2019. A dual Ucp1 reporter mouse model for imaging and quantitation of brown and brite fat recruitment. Mol Metab 20:14–27. [PubMed: 30580967]
6. Lehnig AC, Dewal RS, Baer LA, et al. 2019. Exercise Training Induces Depot-Specific Adaptations to White and Brown Adipose Tissue. iScience 11:425–439. [PubMed: 30661000]
7. Meyer GA, Gibbons MC, Sato E, et al. 2015. Epimuscular Fat in the Human Rotator Cuff Is a Novel Beige Depot. Stem Cells Transl Med 4:764–774. [PubMed: 25999520]
8. Gorski T, Mathes S, Krützfeldt J. 2018. Uncoupling protein 1 expression in adipocytes derived from skeletal muscle fibro/adipogenic progenitors is under genetic and hormonal control. J Cachexia Sarcopenia Muscle 9:384–399. [PubMed: 29399988]
9. Yin H, Pasut A, Soleimani VD, et al. 2013. MicroRNA-133 controls brown adipose determination in skeletal muscle satellite cells by targeting Prdm16. Cell Metab 17:210–224. [PubMed: 23395168]
10. Almind K, Manieri M, Sivitz WI, et al. 2007. Ectopic brown adipose tissue in muscle provides a mechanism for differences in risk of metabolic syndrome in mice. Proc Natl Acad Sci U S A 104:2366–2371. [PubMed: 17283342]
11. Liu W, Liu Y, Lai X, et al. 2012. Intramuscular adipose is derived from a non-Pax3 lineage and required for efficient regeneration of skeletal muscles. Dev Biol 361:27–38. [PubMed: 22037676]
12. Crisan M, Casteilla L, Lehr L, et al. 2008. A reservoir of brown adipocyte progenitors in human skeletal muscle. Stem Cells 26:2425–2433. [PubMed: 18617684]
13. Laurens C, Louche K, Sengenes C, et al. 2016. Adipogenic progenitors from obese human skeletal muscle give rise to functional white adipocytes that contribute to insulin resistance. Int J Obes (Lond) 40:497–506. [PubMed: 26395744]

14. Bryniarski AR, Meyer GA. 2019. Brown Fat Promotes Muscle Growth During Regeneration. J Orthop Res 37:1817–1826. [PubMed: 31042310]
15. Lee C, Liu M, Agha O, et al. 2020. Beige fibro-adipogenic progenitor transplantation reduces muscle degeneration and improves function in a mouse model of delayed repair of rotator cuff tears. J Shoulder Elbow Surg 29:719–727. [PubMed: 31784382]
16. Craft CS, Robles H, Lorenz MR, et al. 2019. Bone marrow adipose tissue does not express UCP1 during development or adrenergic-induced remodeling. Sci Rep 9:17427. [PubMed: 31758074]
17. Lowell BB, S-Susulic V, Hamann A, et al. 1993. Development of obesity in transgenic mice after genetic ablation of brown adipose tissue. Nature 366:740–742. [PubMed: 8264795]
18. Biltz NK, Collins KH, Shen KC, et al. 2020. Infiltration of intramuscular adipose tissue impairs skeletal muscle contraction. J Physiol 598:2669–2683. [PubMed: 32358797]
19. Biltz NK, Meyer GA. 2017. A novel method for the quantification of fatty infiltration in skeletal muscle. Skelet Muscle 7:1. [PubMed: 28073372]
20. Bouxsein ML, Boyd SK, Christiansen BA, et al. 2010. Guidelines for assessment of bone microstructure in rodents using micro-computed tomography. J Bone Miner Res 25:1468–1486. [PubMed: 20533309]
21. Pisani DF, Bottema CD, Butori C, et al. 2010. Mouse model of skeletal muscle adiposity: a glycerol treatment approach. Biochem Biophys Res Commun 396:767–773. [PubMed: 20457129]
22. Melnyk A, Harper ME, Himms-Hagen J. 1997. Raising at thermoneutrality prevents obesity and hyperphagia in BAT-ablated transgenic mice. Am J Physiol 272:R1088–1093. [PubMed: 9140006]
23. Hamann A, Flier JS, Lowell BB. 1996. Decreased brown fat markedly enhances susceptibility to diet-induced obesity, diabetes, and hyperlipidemia. Endocrinology 137:21–29. [PubMed: 8536614]
24. Kitahara T, Li HS, Balaban CD. 2004. Localization of the mitochondrial uncoupling protein family in the rat inner ear. Hear Res 196:39–48. [PubMed: 15464300]
25. Schulz TJ, Huang TL, Tran TT, et al. 2011. Identification of inducible brown adipocyte progenitors residing in skeletal muscle and white fat. Proc Natl Acad Sci U S A 108:143–148. [PubMed: 21173238]
26. Davies MR, Garcia S, Liu M, et al. 2022. Muscle-Derived Beige Adipose Precursors Secrete Promyogenic Exosomes That Treat Rotator Cuff Muscle Degeneration in Mice and Are Identified in Humans by Single-Cell RNA Sequencing. Am J Sports Med 50:2247–2257. [PubMed: 35604307]
27. De Micheli AJ, Laurilliard EJ, Heinke CL, et al. 2020. Single-Cell Analysis of the Muscle Stem Cell Hierarchy Identifies Heterotypic Communication Signals Involved in Skeletal Muscle Regeneration. Cell Rep 30:3583–3595.e3585. [PubMed: 32160558]
28. Petrany MJ, Swoboda CO, Sun C, et al. 2020. Single-nucleus RNA-seq identifies transcriptional heterogeneity in multinucleated skeletal myofibers. Nat Commun 11:6374. [PubMed: 33311464]
29. Sastourné-Arrey Q, Mathieu M, Contreras X, et al. 2023. Adipose tissue is a source of regenerative cells that augment the repair of skeletal muscle after injury. Nat Commun 14:80. [PubMed: 36604419]

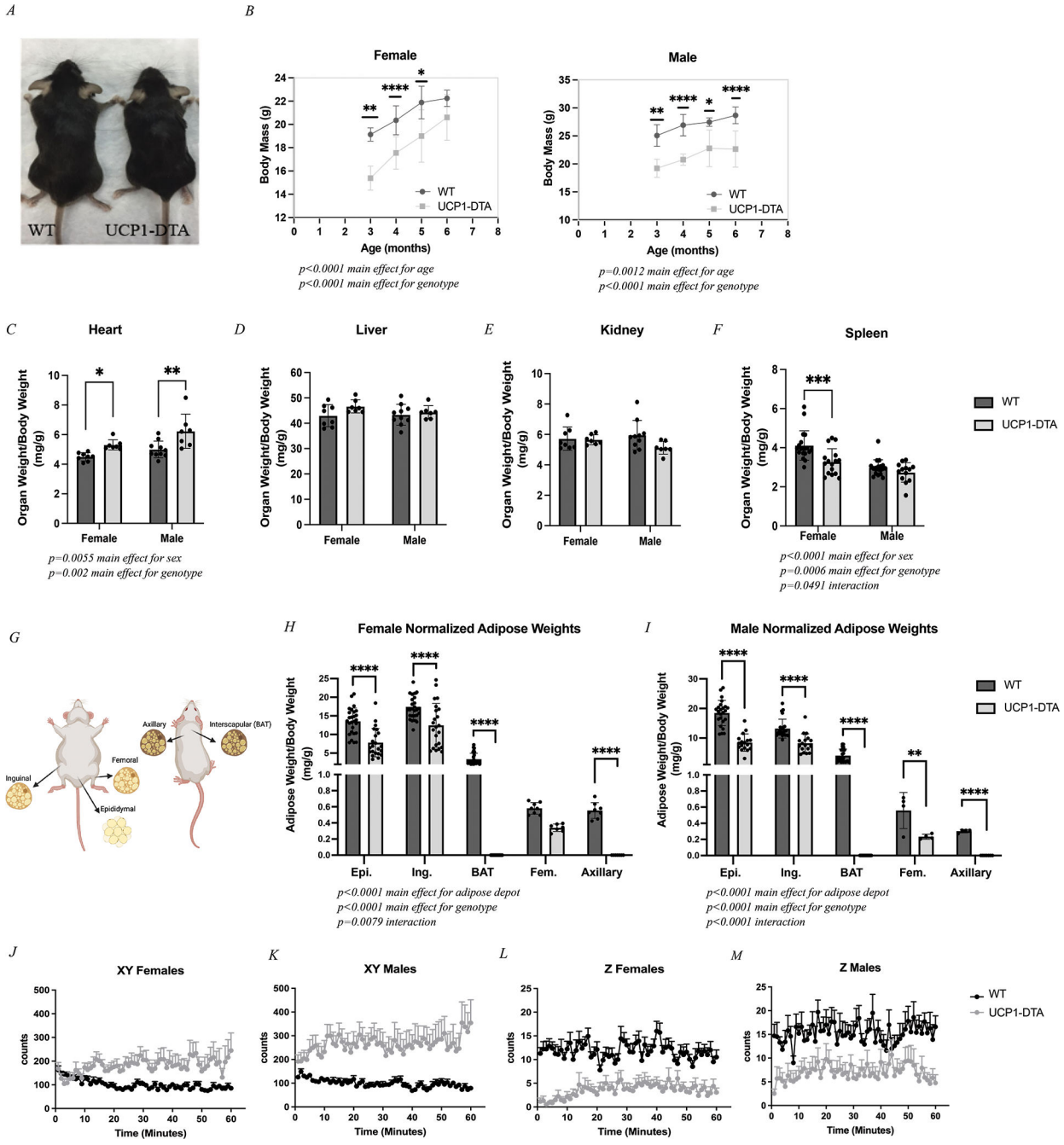

Figure 1. UCP1-DTA Mice Have Reduced Body and Adipose Masses

A Representative image illustrating body size differences between WT mouse (left) and UCP1-DTA mouse (right). *B* Body mass was significantly lower in UCP1-DTA mice across cohort ages. *C* Normalized heart mass is significantly higher in UCP1-DTA mice. *D-E* Liver and kidney analyses show no differences between sex or genotype. *F* Spleen mass was significantly reduced in female mice only. *G* Graphical anatomical depiction of six adipose depots including three classical fat depots: Epididymal (Epi.), Inguinal (Ing.), and interscapular (BAT) and two previously identified epi-muscular fat depots including Femoral (Fem.) and Axillary adipose tissue. *H* Normalized adipose masses in female mice show main

effects for adipose depot and genotype with specific differences noted between Epi, Ing., BAT, and Axillary depots. *I* Normalized adipose masses in male mice demonstrate main effects for adipose depot and genotype with specific differences noted across all five fat depots between genotypes. *J-M* Activity data in WT and UCP1-DTA female and male mice shows that in XY directions, UCP1-DTA mice are significantly more active than WT mice, but significantly less active in the Z direction. Data are presented as mean ± SD. *P<0.05, **P<0.01, ***P<0.001, ****P<0.0001. Statistical significance set at p<0.05. Analyses were in Prism using two-way ANOVA or multiple, independent t-tests, or linear regression.

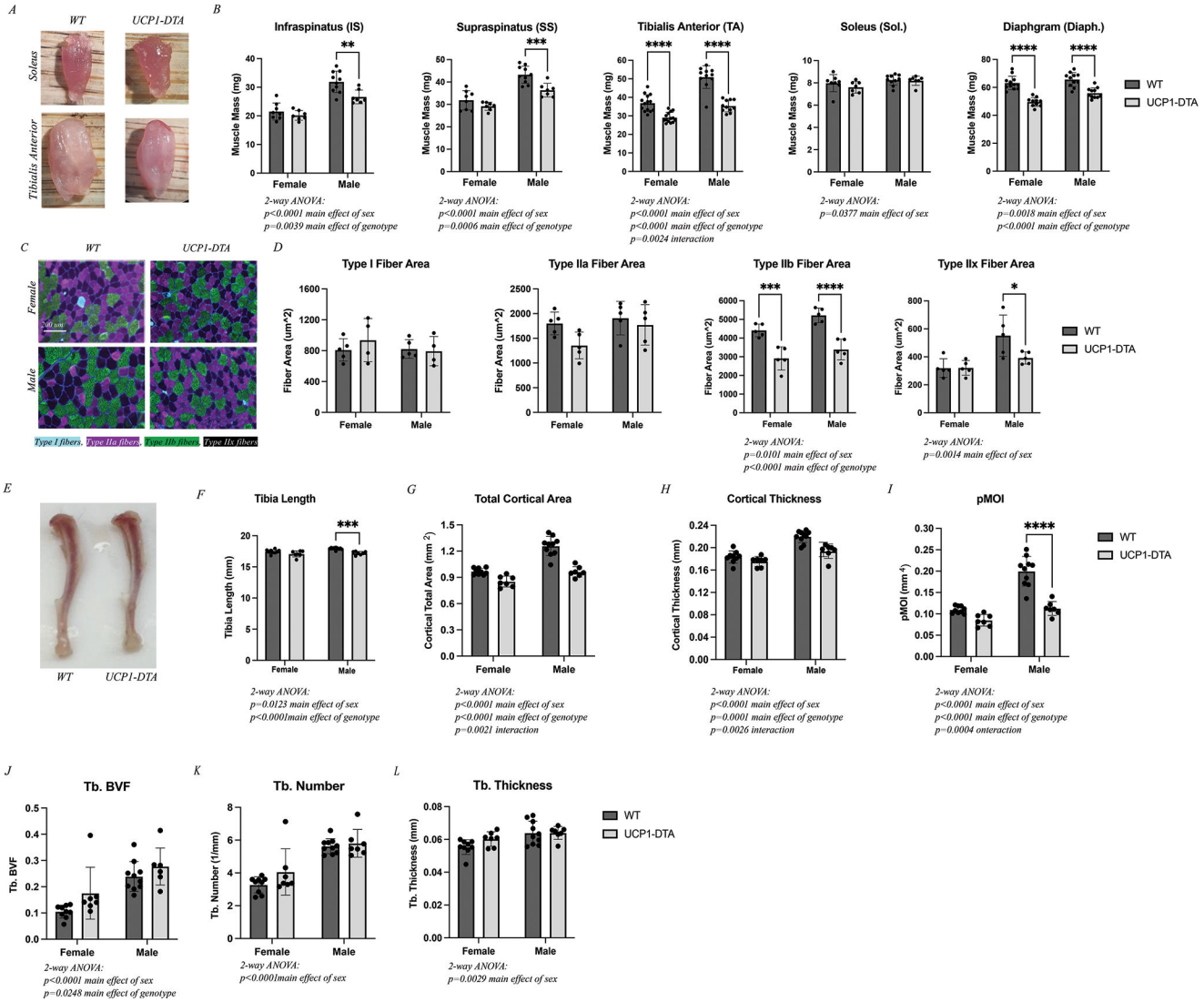

Figure 2. UCP1-DTA Mice Show Altered Skeletal Muscle and Bone Growth

A Images of WT and UCP1-DTA soleus and tibialis anterior (TA) muscles illustrate gross size differences in the TA, but not the soleus. *B* Raw muscle masses harvested from female and male WT and UCP1-DTA mice including infraspinatus (IS), supraspinatus (SS), tibialis anterior (TA), soleus (Sol.), and diaphragm (Diaph.) demonstrating reduced mass in all but soleus muscles. *C* Representative 20x images of TA muscles from both female and male WT and UCP1-DTA immunostained against myosin heavy chain isoforms to detect specific fiber types. Type I fibers: Cyan, Type IIa: Magenta, Type IIb: Green, and Type IIx: Black/No channel. Scale bar represents 200 μm. *D* Analysis of fiber area by fiber type found a significant reduction in type IIb fiber area in UCP1-DTA males and females and type IIx fibers in males only. *E* Representative tibia bone images illustrate a small decrease in length in UCP1-DTA mice. *F* Analysis of tibia length with male WT mice have significantly longer tibias than UCP1-DTA males. *G-I* Total cortical area, cortical thickness and pMOI are modestly reduced in UCP1-DTA mice compared with WT. *J-L* Ttrabecular (Tb.) bone volume fraction (BVF), Tb. Number and Tb. Thickness are similar between UCP1-DTA and

WT male and female mice. N=8–12. Data are presented as mean ± SD. *P<0.05, **P<0.01, ***P<0.001, ****P<0.0001. Statistical significance set at $p<0.05$. Analyses were in Prism using two-way ANOVA or multiple, independent t-tests.

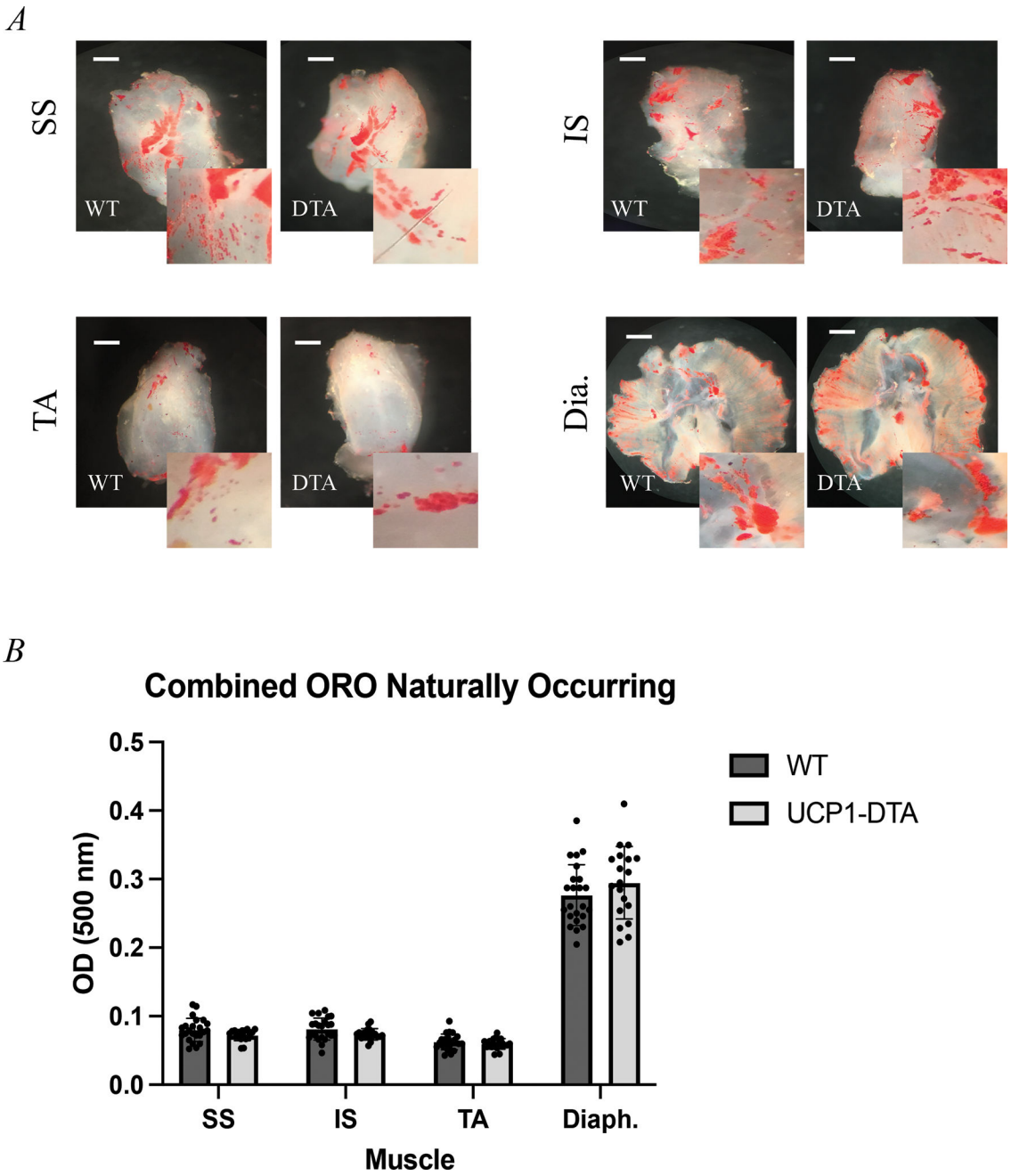

Figure 3. Intramuscular Adipose Tissue (IMAT) Develops Without UCP-1-Expressing Cells

Oil Red O staining of decellularized *A* Supraspinatus (SS), Infraspinatus (IS), Tibialis Anterior (TA), and Diaphragm (Dia.) muscles depicting visually similar amounts of naturally occurring IMAT (red) in both wild type (WT) and UCP1-DTA genotypes. *B* Optical density (OD) measurement confirms similar amount of lipid content across the four muscles in both female (n=14) and male (n=13) mice. Scale bar 1mm. Analysis performed in Prism using multiple, independent t-tests. Statistical significance set at $p<0.05$.

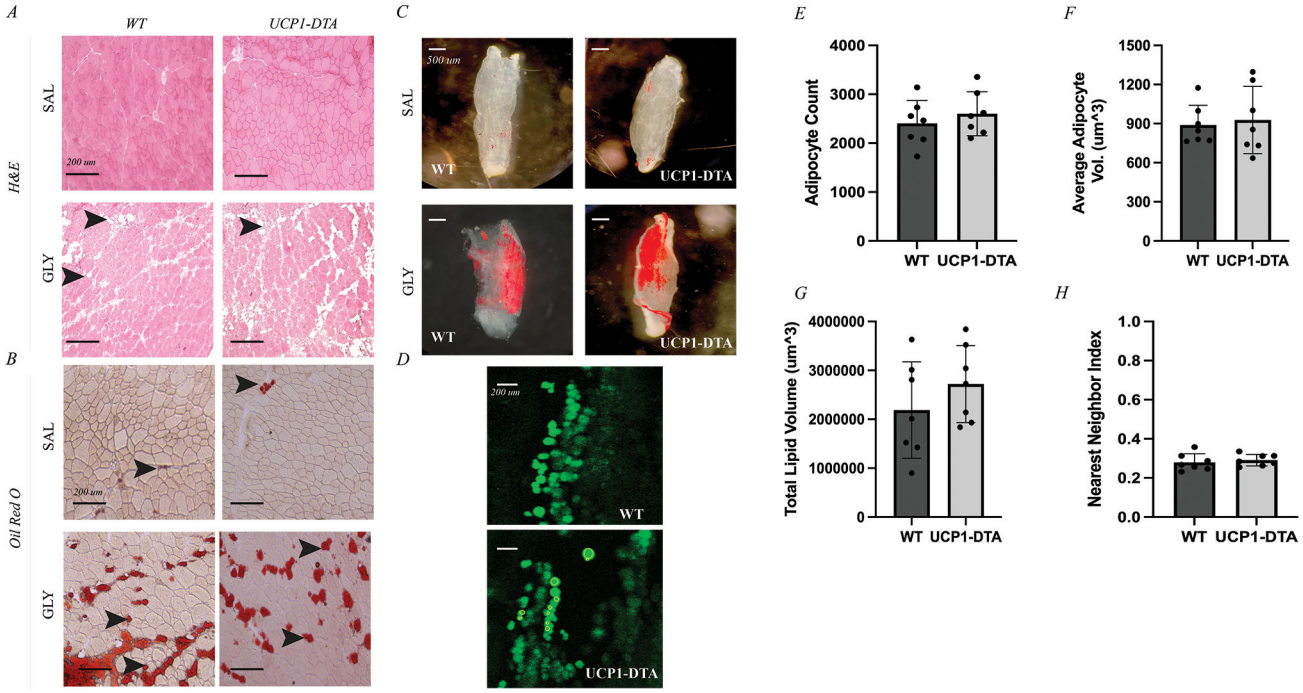

Figure 4. Glycerol-Induced IMAT Develops Without UCP-1-Expressing Cells

A Hematoxylin and Eosin (H&E) staining of tibialis anterior (TA) muscle after 14 days of either saline (SAL) or glycerol (GLY) treatment shows extensive appearance of intramuscular adipocytes (IMAT) in GLY groups represented by white, globular structures (black arrows). *B* Oil Red O (ORO) staining of TA muscles identifies these intramuscular adipocytes as lipid filled (black arrows). *C* Oil Red O staining of decellularized EDL muscles of both wild type (WT) and UCP1-DTA genotypes injected with saline showing minimal IMAT (red) or injected with glycerol causing IMAT accumulation in similar amount between genotypes (red). Scale bars for A and B 1 mm. *D* Sample slices of EDLs treated with glycerol and stained with BODIPY and visualized using confocal microscopy in WT and UCP1-DTA mice. Individual adipocytes are identified as individual green circular regions of interest. *E* Quantification of adipocyte metrics via confocal microscopy in male WT and UCP1-DTA mice (n=21) showing similar average adipocyte count between genotypes in response to glycerol injection. *F* Average adipocyte volume similar in WT and UCP1-DTA mice. *G* Total lipid volume of WT and UCP1-DTA mice are similar with glycerol injection. *H* Nearest neighbor index as a measure of spatial clustering of intramuscular adipocytes show similar clustering between WT and UCP1-DTA mice. Data are presented as mean ± SD. Analysis performed in Prism using independent t-tests. Statistical significance set at $p<0.05$.

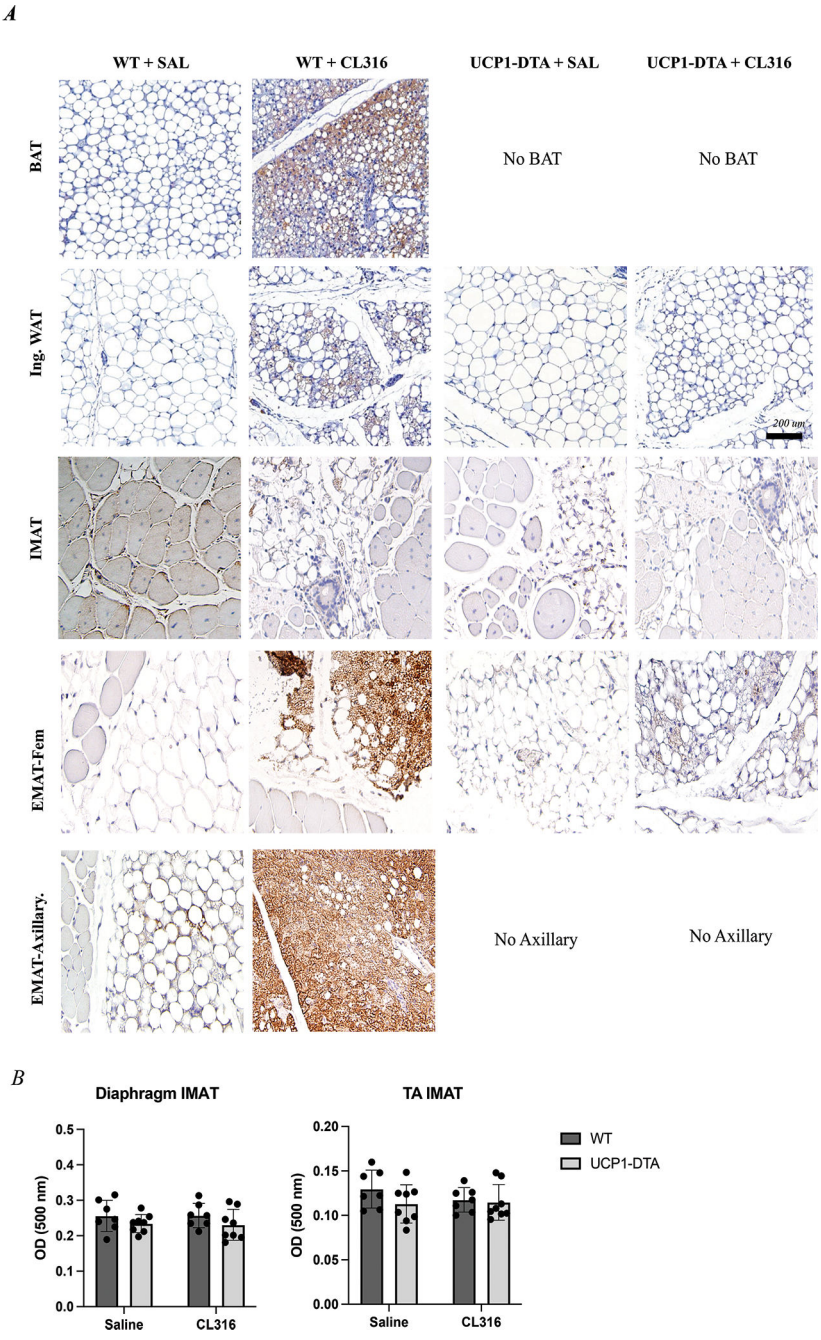

Figure 5. Effects of Beiging on Adipose Depots

A) Representative images from UCP-1-immunostained adipose depots *Row 1* In WT micce, brown adipose (BAT) adipocytes have multilocular morphology, and increased UCP-1 immunostaining intensity with CL316,243 (β3 adrenergic agonist) treatment (brown). UCP1-DTA mice completely lack the classical interscapular, BAT depot. *Row 2* Inguinal white adipose (Ing. WAT) has interspersed unilocular and multilocular adipocytes in saline (SAL) treated mice with increased UCP-1+ multilocular cells following CL316 treatment in WT, but less so in UCP1-DTA. *Row 3* Tibialis anterior (TA) muscles of both WT and UCP1-DTA genotypes injected with glycerol show deposition of IMAT across all genotypes

and conditions noted by unilocular adipocytes. Both WT and UCP1-DTA mice treated with CL316 show small localized UCP-1+ cells, however, to a much lesser extent than Ing. WAT. *Row 4* Femoral Epi-muscular adipose depots (Fem. EMAT) from WT and UCP1-DTA mice show predominantly large, unilocular lipid droplets in saline-treated conditions. WT and UCP1-DTA Fem. EMAT treated with CL316 show a dramatic increase in the intensity of UCP-1 immunostaining. *Row 5* Similar to Ing. WAT, Axillary EMAT have interspersed unilocular and multilocular adipocytes in saline-treated condition, and when treated with CL316 have dramatically higher UCP-1 staining intensity. *B* There are no changes in total IMAT quantity in response to CL316 treatment in either diaphragm (Diaph.) or glycerol-treated TA in response to CL316. N= 8–19. Data are presented as mean ± SD. *P<0.05, **P<0.01, ***P<0.001, ****P<0.0001. Statistical significance set at $p<0.05$. Analyses were in Prism using two-way ANOVA. Scale bar is 200 μm.